Diluting & mixing at the nanoscale for Organ-on-a-chip applications

Author: Carla Parcerisas Padilla
Facultat de Física, Universitat de Barcelona, Diagonal 645, 08028 Barcelona, Spain.

Advisor: Carolina Rodríguez-Gallo, Anna M. Vilà Arbonès

Abstract: In this project, we designed, fabricated, and characterized a serpentine-shaped organ-on-a-chip (OoC) device. The device aims to model the effects of non-alcoholic steatohepatitis (NASH) on muscle tissue. A $6 \cdot 10^{-3}\ mg \cdot mL^{-1}$ dilution of Rhodamine B fluorophore in MilliQ water was used to simulate liver medium, while Milli-Q water represented the muscle medium. Mixing efficiency was evaluated under different inlet liver pressures using fluorescence microscopy and Gaussian fitting of intensity profiles. The results showed that lower inlet pressures improved mixing, consistent with theoretical predictions for laminar flow regimes. Complete homogenization was observed immediately before the muscle chamber. Experimental limitations, such as unfocused images and fluorescence background from tubing, affected data quality. Nevertheless, with improved techniques, this device could be fully characterized.
Keywords: Microfluidics, Organ-on-a-chip, Laminar flow, Fluorescence imaging, Data Analysis,
SDGs: Good Health and Well-Being, Quality Education

I. INTRODUCTION

Organ-on-chip devices, fabricated using microchip technologies, operate at the microscale and simulate key aspects of human organ physiology by replicating simplified functional units [1]. In this study, we developed an OoC system to investigate sarcopenia (progressive loss of skeletal muscle mass and function) induced by non-alcoholic steatohepatitis (NASH), a liver disease characterized by fat accumulation, steatotic hepatocytes, and activated hepatic stellate cells (HCs) [2].

To study how diseased liver cells affect muscle tissue, our OoC consists of two chambers, one for liver cells and another for muscle cells. Previous experiments showed that non-diluted liver medium is toxic for skeletal muscle, necessitating dilution and mixing with the muscle medium before it arrives in the muscle chamber.
At the microscale, this mixing occurs primarily via molecular diffusion, a statistical process in which molecules move from high to low concentration regions, leading to gradual homogenization of the liquids [3]. Efficient mixing over short distances and within minimal time is crucial to optimize chip design and performance.

Micromixers are generally divided into two categories: active and passive micromixers.
Active micromixers typically offer higher mixing efficiency but require more complex fabrication methods. Passive micromixers, by contrast, are simpler to manufacture and operate as they only require the input pressure to drive the flow.
In passive micromixers, mixing depends on molecular diffusion, influenced by the diffusion coefficient, interfacial surface area, and concentration gradient. To improve mixing, the design strategy focuses on increasing this interfacial surface area and modifying the channel geometry (e.g., adding loops to induce chaotic advection)[4][5].

II. MICROSCALE FLUID PHYSICS

Microfluidics is the science of fluid flow on small scales where flows in microchannels are typically characterized by low Reynolds numbers. This implies that viscous forces dominate over inertial forces, resulting laminar flow [3].

In this section, we present the fundamental principles and governing equations of microfluidic flow to provide the mathematical background for experimental work.
Microfluidic flows are governed by the Navier-Stokes equations. Fluids are approximated as incompressible (constant density, ρ). The general form of the equation is[4][6]:

$$\rho\frac{\partial\vec{u}}{\partial t} + \rho(\nabla\vec{u})\vec{u} = -\vec{\nabla}p + \rho\vec{g} + \eta\nabla^2\vec{u} \tag{1}$$

where $\mathbf{u} = \mathbf{u}\ (\vec{r}, t)$ is the velocity of the fluid [m s^{-1}]; ρ is the fluid density [kg m^{-3}]; η is the viscosity [Pa s]; $\vec{g}$ is the gravitational acceleration vector [m s^2] and p is the pressure [Pa].

Now consider a channel aligned along the x-direction. Assuming the fluid is incompressible, unidirectional, steady, and Newtonian, the equation (1) simplifies to [6]:

$$\vec{\nabla}p = \eta\nabla^2\vec{u} \tag{2}$$

This equation can be solved to obtain the velocity profile, which reveals that velocity along a straight channel follows a parabolic distribution, reaching its maximum at the center of the channel.
By spatially integrating this velocity profile, we obtain the flow rate, which follows Hagen-Poiseuille's law:

$$Q = \frac{\Delta p}{R_H} \tag{3}$$

Here, R_H is the hydraulic resistance, which depends on the geometry of the channel (in our case, rectangular cross-section).

The key implication of this equation is that the flow rate is proportional to the pressure difference along the channel. Thus, injecting a higher pressure results in a higher maximum velocity at the center of the channel[6].

III. EXPERIMENTAL METHODS

A. Device design

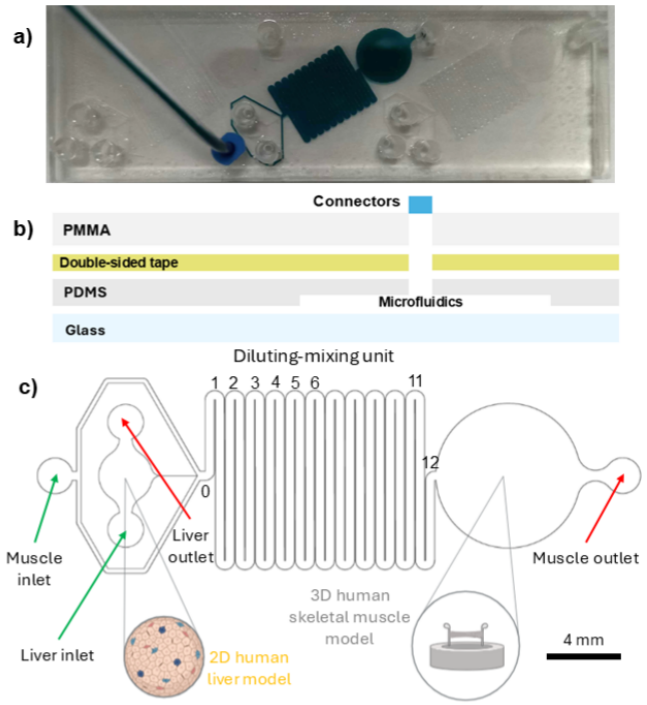

FIG. 1: (a) Top view of assembled chip. Blue ink was injected into the middle device to facilitate the visualization of the fluidic channel. (b) Schematics of chip layers. (c) Microfluidic part showing both types of cells in their respective chambers, as well as the inlet and outlet connections. The numbers indicate the locations from which data were obtained.

Each chip contains three replicas of the same device with one diluting mixing unit each FIG. 1(a). The final device consists of three different layers (FIG. 1(b)). The bottom layer is a standard microscope glass slide of 75.5 X 25 mm, with a thickness of 1 mm, to allow the visualization of the channels with a standard optical microscope. The middle layer is fabricated from PDMS, a biocompatible silicon-based polymer. The top layer is made of PMMA, a synthetic polymer derived from methyl methacrylate, which serves as the interface for tube connectors.
The PDMS layer is bonded to the glass using plasma treatment and to the PMMA using a double-sided adhesive tape with a thickness of 170 μm to avoid leaks.

As shown in FIG. 1(c), the microfluidic design, with a constant chamber/channel height of 100 μm, includes the liver chamber with a diameter of 3 mm, positioned adjacent to the inlet and outlet connectors of the liver medium. Emerging from the liver chamber is a primary channel with a width of 10 μm. Above the liver chamber is the muscle medium inlet, which is connected to two outlet channels, each with a width of 250 μm. These two channels eventually merge at an intersection point with the outlet channel from the liver chamber, resulting in a double mixing interface surface area, that enhances mixing efficiency.
Following the intersection lies the mixing unit, which consists of a channel with a width of W = 510 μm, where fluids from both sources mix. The mixing unit terminates in the muscle chamber, which has a diameter of 8 mm and includes the outlet for the muscle medium.

The mixing unit has a serpentine design consisting of 11 upper loops and 11 lower loops.
In straight channels, the flow follows a Poiseuille profile: a parabolic velocity distribution with the maximum velocity value at the centerline. In curved channels (loops), however, the centrifugal force causes the velocity maximum to shift toward the concave outer wall. As a result, the center of the channel, where the interface between the two different liquids typically lies, experiences a lower axial velocity, allowing molecules more residence time for molecular diffusion to occur.
Additionally, the shift of the maximum velocity toward the outer wall creates a high pressure gradient between the location of the maximum velocity and the other wall of the channel. This pressure difference drives a transverse secondary flow, forming Dean vortices. These vortices are perpendicular to the primary flow direction. This enhances mixing, as molecules from both liquids move and mix throughout the transversal plane of the channel [5].

B. Chip fabrication

The diluting-mixing unit was designed using AutoCAD and fabricated on a 5-inch silicon wafer via standard photolithography. The wafer was first dehydrated at 200°C for 15 minutes and treated with oxygen plasma for 30 seconds to improve photoresist adhesion.

Next, a SU-8 2010 interlayer was spin-coated onto the wafer (500 rpm for 10 seconds, then 3000 rpm for 60 seconds), soft-baked at 95°C for 6 minutes, flood-exposed to 140 $mJ\ cm^{-2}$ of UV light without a photomask, rested for 10-minutes to allow complete photoreactions, and a post-exposure baked at 65°C for 1 minute and at 95°C for 3 minutes.

Following this, the SU-8 2100 structural layer was spin-coated twice (500 rpm, then 3500 rpm) to obtain

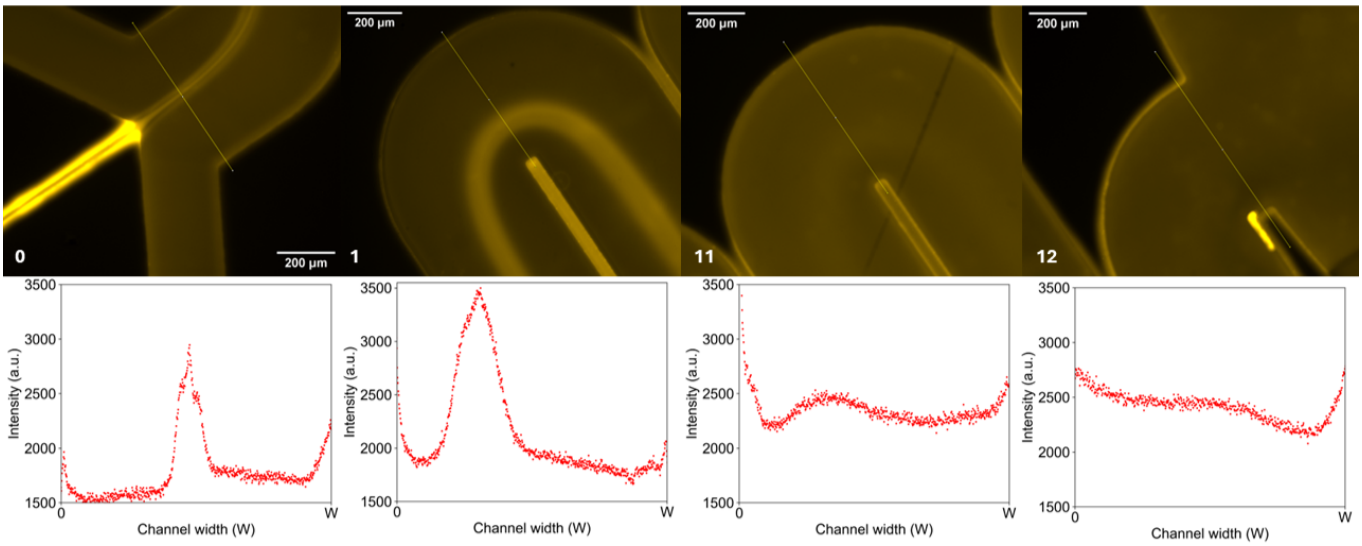

FIG. 2: Four microscopy images taken at an inlet liver pressure of 300 $mbar$, along with the corresponding intensity profiles. A white number is shown at the lower left part of each microscopy image, indicating its location in the diluting-mixing unit (see FIG.1).

a 100 μm thickness. Soft-baking was performed at 65°C for 5 minutes and then 95°C for 20 minutes. The microfluidic pattern was transferred onto the wafer by exposing it to 300 $mJ\ cm^{-2}$ of UV light through an acetate photomask. After 10-minutes resting period, a post-exposure bake was conducted at 65°C for 5 minutes and at 95°C for 20 minutes. Development was performed in propylene glycol monomethyl ether acetate for 15 minutes to dissolve unexposed SU-8. A final rinse with isopropanol and nitrogen gas drying completed the process.
Finally, the mold was silanized in a vacum chamber with a drop of Silane (SiH_4) for at least one hour to facilitate polydimethylsiloxane (PDMS) demolding.

The wafer was then placed in a petri dish covered with a layer of PDMS, a biocompatible silicon-based polymer composed of a base and a curing agent (50 g base: 5 g curing agent). The mixture was degassed and cured for 4 h at 65°C. All components were cleaned before assembly [7]. The complete chip is shown in FIG. 1(a).

C. Experimental setup

For the mixing study, we conducted a principal experiment in which the chip was connected to a pressure pump to control the injection pressure of both liquids (see FIG. S1). Flow behavior was observed via fluorescence microscopy, and intensity data were collected from various regions of the chip (FIG. 2). The experiment was repeated using different inlet pressures of the liver medium, ranging from 250 to 500 $mbar$. The liver medium was simulated using Rhodamine B solution at a concentration of $6 \cdot 10^{-3}\ mg \cdot mL^{-1}$.
Images were acquired using a 10x microscope objective, with a light intensity setting of 75.7% and an exposure time of 500 ms. Rhodamine B was chosen as it emits yellow fluorescence and has a diffusion coefficient similar to that of ribosomes or small proteins[4]. Milli-Q water was used to simulate the muscle medium.

To determine the appropriate concentration of the Rhodamine B solution, a preliminary calibration was performed using solutions ranging from $4 \cdot 10^{-4}\ mg \cdot mL^{-1}$ to $4\ mg \cdot mL^{-1}$. These solutions were imaged in a 96-well plate under identical microscopy conditions (6.1 % light intensity, 150 ms exposure).
The images were then analyzed with ImageJ, which calculated the average pixel intensity for each well. The resulting intensity values were plotted against Rhodamine B concentration (see FIG. S2(a)).
Our objective was to identify the linear region, as shown in FIG. S2(b), as it avoided the effects of self-quenching, a phenomenon in which, at high concentrations, fluorescent molecules reduce their own emission intensity due to their proximity, causing energy transfer between nearby molecules instead of light emission [8].
Based on this analysis, we selected a final working concentration of $6 \cdot 10^{-3}$ mg mL^{-1}.

D. Mixing efficiency analysis

The objective of the mixing analysis was first to evaluate whether the two liquids were fully mixed before reaching the muscle chamber and second, to determine which inlet pressure led to faster mixing.

For the mixing efficiency analysis, microscopy images were taken at different positions along the mixing unit (see FIG. 1). The intensity was measured along a defined

cross-sectional line at each location, and the resulting intensity profiles were plotted as a function of channel width, FIG. 2.
As these profiles exhibited a Gaussian distribution shape, we used a custom-made Python script and extracted the standard deviation (σ) from each fit. These σ values were then used to calculate the mixing index, defined as[4]:

$$\gamma = 1 - \frac{\sigma_{min}}{\sigma} \tag{4}$$

where σ_{min} is the standard deviation corresponding to the unmixed condition at the intersection (Location 0). The mixing index ranges from 0 to 1, with a value approaching 1 indicating perfect mixing. In this case, the intensity profile should become flat, meaning $\sigma \to \infty$.

The second analysis performed was to compare the intensity in the liver and muscle chambers under different applied pressures. The intensity difference between the two chambers was plotted as a function of pressure. This analysis allowed us to study the diluting performance of our device depending on the injected pressure. Since different intensities translate to differences in Rhodamine B concentrations.
The intensity values were obtained using the same procedure as in the calibration experiment.

In the first analysis, three different experiments were used at each pressure value, allowing us to calculate statistical errors with N = 3.
In the second analysis, some experiments were conducted with N≠ 3. While errors were also calculated statistically, the sample size N varied in some cases.

IV. RESULTS

FIG. 3 shows the mixing index, calculated using equation (4), at positions marked in FIG. 1. The plot indicates that higher inlet liver pressures, especially at 500 *mbar*, result in lower mixing efficiency, as the mixing index converges more slowly toward 1 at this pressure.

This observation aligns with theoretical expectations. As is well known, the flow within the microfluidic chip is laminar, causing a parabolic velocity profile in straight channels, with the maximum velocity at the center of the channel. In the middle of the channel, the Rhodamine B flow is in contact with the Milli-Q water flow.
Under laminar flow conditions, mixing is primarily governed by molecular diffusion. Therefore, the efficiency of mixing depends on the time available for molecules to diffuse. When a higher inlet liver pressure is applied, the fluid velocity increases, reducing the time available for diffusion[6]. As a result, the mixing index approaches 1 more slowly at higher inlet pressures. This is clearly visible in FIG. 3

Additionally, an asymptotic fit constrained to approach 1 was applied to the data in order to evaluate whether the fluids at each inlet liver pressure tend

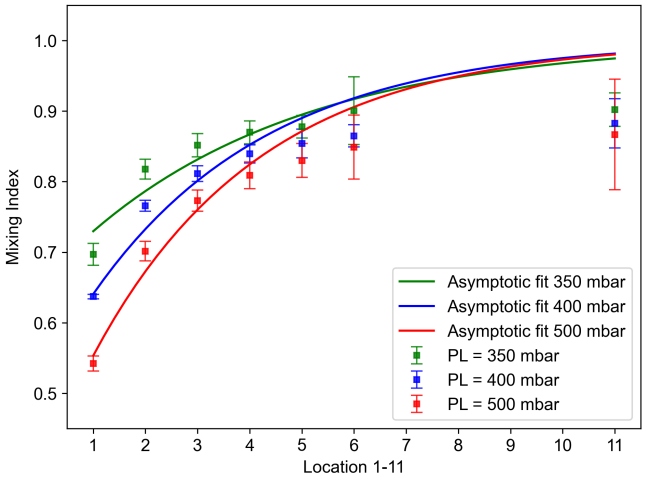

FIG. 3: Mixing Index data with corresponding error bars, obtained from Gaussian fits of intensity plots at three different inlet liver pressure values. Positions 1-11 correspond to the locations labelled in FIG.1. The asymptotic fits are constrained to approach a value of 1.

toward complete mixing (mixing index approaching 1). As shown in the plot, the error bars for nearly all data points fall within the bounds of the asymptotic fit.
The last data point deviates more from the asymptotic fit due to difficulties in performing an accurate Gaussian fit.

As shown in FIG. 4, the intensity profiles become flat at position 12 from FIG. 1, indicating that the fluids are already mixed before entering the muscle chamber.
The flat profile indicates that IMAGE J measured nealry uniform intensity values across all pixels along the analyzed line.

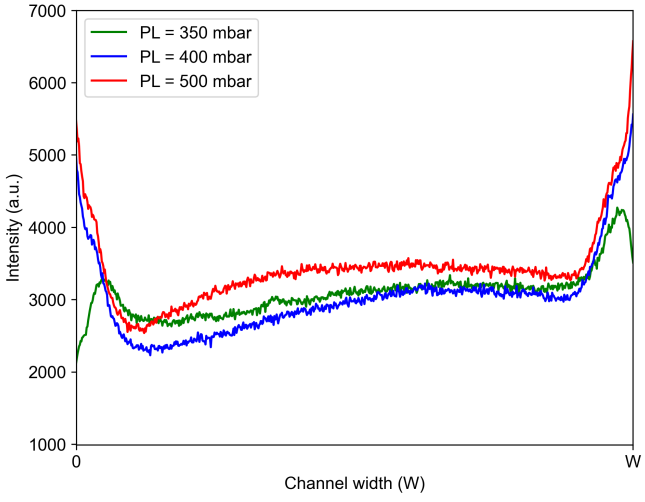

FIG. 4: Intensity profile at the final location of the chip before the mixture enters the muscle chamber, for three different inlet liver pressure values.

Finally, FIG. 5 presents the difference in intensity between the liver and muscle chambers as a function of the inlet liver pressure. According to the calibration study, within a certain concentration range of Rhodamine B, the intensity is proportional to the concentration; higher intensity means higher concentrations, and lower intensity means lower concentrations.

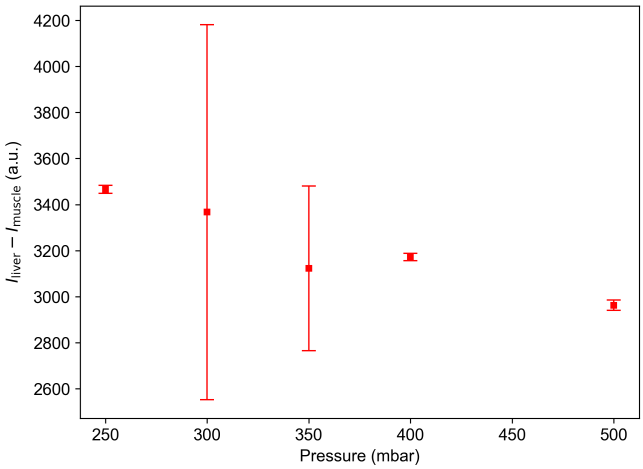

FIG. 5: Difference between the intensity in the liver chamber and the intensity in the muscle chamber, with corresponding error bars, plotted as a function of the inlet liver pressure.

The intensity values measured in the liver chamber should remain constant regardless of pressure, as mixing has not yet occurred.
The graph shows that the intensity difference decreases as the inlet liver pressure increases. This implies that the intensity decreases more significantly from the liver chamber to the muscle chamber when the inlet pressure is lower. Since fluorescence intensity is proportional to the concentration of Rhodamine B (FIG. S2(b)), a greater intensity difference indicates a larger concentration difference, meaning the fluid in the muscle chamber is more diluted at low inlet pressures.
Notably, the large error bars observed at 300 and 350 *mbar* are attributed to significant variability in the intensity values obtained from the muscle chamber across different experiments. This variability likely results from differences in pixel-level intensity, meaning that the average intensity value provided by ImageJ has a high standard deviation, leading to inconsistent measurements between replicates.

V. CONCLUSIONS

In this study, we fabricated an organ-on-a-chip incorporating a serpentine diluting mixing unit and a double interface surface area. Furthermore, we analyzed the mixing efficiency and aimed to identify the position of complete homogenization of the fluids.

Our results demonstrate that a lower inlet liver pressure allows better mixing efficiency, which is in good agreement with theoretical predictions [6].
Although the mixing index remained below one in all the tested scenarios, the intensity plots from the region immediately before the muscle chamber appear nearly flat, suggesting uniform intensity across the width of the channel.

However, several experimental limitations may have affected the precise identification of the complete mixing point. First, the complex setup required numerous tubing connections to both the pump and the chip. Occasionally, the tubes connected to the chip, carrying Rhodamine B, were positioned too close to the objective lens and were inadvertently captured in the fluorescence images. This sometimes caused artificially elevated intensity readings. Additionally, some fluorescence images were slightly unfocused, complicating Gaussian fitting during data analysis.

Nevertheless, through the experience gained during this study, we anticipate that improvements in our experimental techniques will enhance measurement accuracy and could eventually identify the precise conditions for complete mixing in future work.

Acknowledgments

I would like to thank the Institute of Bioengineering of Catalonia (IBEC) for this opportunity, and especially my advisor, Dra. Carolina Rodriguez-Gallo for her support and guidance during this work. I would also like to thank Dra. Anna M. Vilà Arbonès for her help as my advisor at the University of Barcelona. And to my friends and family, who cheered me on, lifted me up, and never let me doubt myself.

[1] S. N. Bhatia and D. E. Ingber, *Nat. Biotechnol.,* vol. 32, 2014.
[2] C.-H. Liu and G. Habig, *Res. Gate,* 2025.
[3] S. Seiffert, *Microfluidics: Theory and Practice,* De Gruyter Graduate, 2020.
[4] Y. Liao, M. Yves, and B. Lassalle-Kaiser, *Sci. Rep.*, vol. 11, 2021.
[5] Y. Saffar and S. Kashanj, *Micromachines*, vol.14, 2023.
[6] K. W. Oh, K. Lee, B. Ahn and E.P. Furlani, *Lab Chip*, vol.12, 2012.
[7] A. P. Antonov, M. Terkel, F. Schwarzendahl, C. Rodríguez-Gallo, P. Tierno and H. Löwen, *Commun. Phys.*, vol. 8, 2025.
[8] D. Setiawan, A. Kazaryan, M.A. Martoprawiro and M. Filatov, *Phys. Chem. Chem. Phys.*, vol. 12, 2010.

Dilució i mescla a nanoescala per a aplicacions en Organ-on-a-xip

Author: Carla Parcerisas Padilla
Facultat de Física, Universitat de Barcelona, Diagonal 645, 08028 Barcelona, Spain.

Advisor: Carolina Rodríguez-Gallo, Anna M. Vilà Arbonès

Resum: En aquest projecte, hem dissenyat, fabricat i caracteritzat un dispositiu òrgan-en-xip amb forma de serpentina. L'objectiu del dispositiu és modelar els efectes de l'esteatosi hepàtica no alcohòlica sobre el teixit muscular. Per simular el medi del fetge s'ha utilitzat una dilució de $6 \cdot 10^{-3}$ $mg \cdot mL^{-1}$ de fluoròfor Rodamina B en aigua Milli-Q, mentre que el medi muscular s'ha representat amb aigua Milli-Q. L'eficiència de barreja s'ha avaluat sota diferents pressions d'entrada la dilució de Rhodamina B mitjançant microscopia de fluorescència i ajustos gaussians dels perfils d'intensitat. Els resultats mostren que les pressions d'entrada més baixes milloren l'eficiència de la barreja, en línia amb les prediccions teòriques per a règims de flux laminar. S'ha observat una homogeneïtzació completa just abans de la cambra muscular. Limitacions experimentals com imatges desenfocades i fons de flourescència procedent dels tubs, han afectat a la qualitat de les dades. No obstant això, amb una millora de les tècniques experimentals, aquest dispositiu podria ser completament caracteritzat.
Paraules clau: Microfluidica, Flux laminar, Organ-on-a-chip, Microscopia de fluorescència, Anàlisi de dades
ODSs: Salut i benestar, Educació de qualitat

Objectius de Desenvolupament Sostenible (ODSs o SDGs)

1. Fi de la es desigualtats		10. Reducció de les desigualtats	
2. Fam zero		11. Ciutats i comunitats sostenibles	
3. Salut i benestar	X	12. Consum i producció responsables	
4. Educació de qualitat	X	13. Acció climàtica	
5. Igualtat de gènere		14. Vida submarina	
6. Aigua neta i sanejament		15. Vida terrestre	
7. Energia neta i sostenible		16. Pau, justícia i institucions sòlides	
8. Treball digne i creixement econòmic		17. Aliança pels objectius	
9. Indústria, innovació, infraestructures			

El contingut d'aquest TFG, part d'un grau universitari de Física, es relaciona amb l'ODS 4, i en particular amb la fita 4.4, ja que contribueix a l'educació a nivell universitari. També es pot relacionar amb l'ODS 3 ja que aquesta ODS ens impulsa a prevenir i combatre diverses malalties.

Appendix A: SUPPLEMENTARY MATERIAL

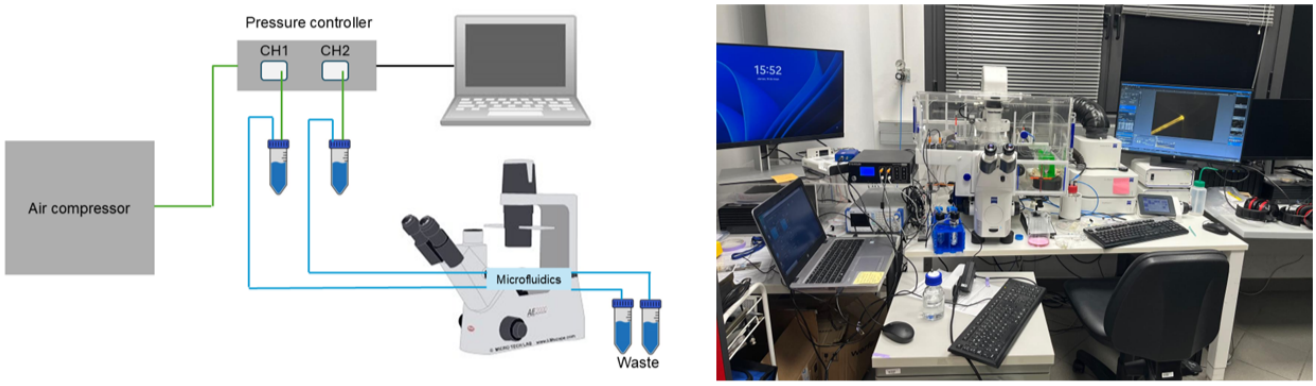

FIG. 6: **Supplementary 1.** (a) Schematics of the experimental setup. Green lines represent air connections, blue lines represent liquid connections, and black lines represent electrical connections. (b) Photograph of the experimental setup.

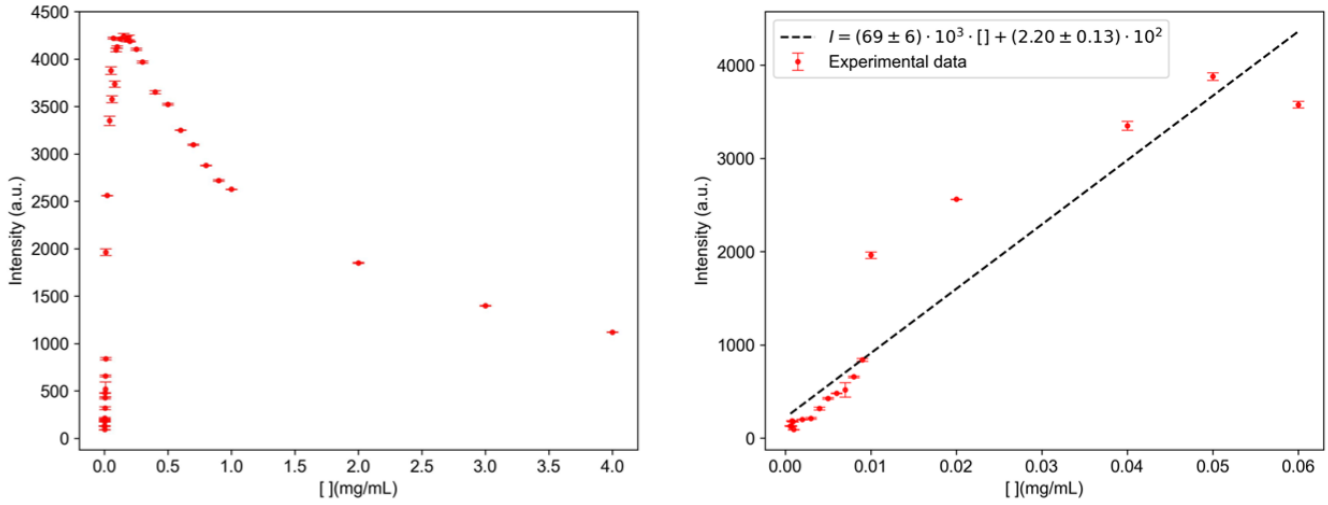

FIG. 7: **Supplementary 2.** (a) Measured intensity (a.u.) versus Rhodamine B concentration ($mg \cdot mL^{-1}$) showing self-quenching starting from the maximum intensity at concentrations around 0.5 $mg \cdot mL^{-1}$. (b) Linear region of (a) with the corresponding linear regression plotted alongside the experimental data.